Microfluidics and Nanofluidics (2018) 22:35
https://doi.org/10.1007/s10404-018-2054-4

SHORT COMMUNICATION

A temperature-based diagnostic approach for paper-based microfluidics

A. Terzis[1] · G. Yang[1] · I. Zarikos[2] · E. Elizalde[3] · B. Weigand[1] · A. Kalfas[4] · X. Ding[5]

Received: 15 November 2017 / Accepted: 3 March 2018 / Published online: 10 March 2018

Abstract
We present the potential of a quantitative temperature-based diagnostic approach for paper-based microfluidics, extending the work of Terzis et al. (J Colloid Interface Sci 504:751–757, 2017) which demonstrated a significant heat release at the liquid front during capillary-driven flows in cellulosic materials. Here, we investigate the applicability of biological fluids to provide a temperature rise at the imbibition front, and successfully demonstrate a monotonic trend between the level of local temperature rise and the concentration of specific analytes. In addition, effects of paper thickness and width are also examined.

Keywords Paper-based microfluidics · Quantitative diagnostics · Capillary thermodynamics

1 Introduction

Microfluidics have a great potential for biomedical applications (Yager et al. 2006) and in 2007, patterned paper has been proposed as a substrate material resulting in a low-cost and portable bioassay (Martinez et al. 2007). Since their establishment as a medical diagnostic tool (Martinez et al. 2010), microfluidic paper-based analytical devices (μPADs) initiated a new class of inexpensive and easy-to-use point-of-care diagnostics for the developing world (Yetisen et al. 2013; Cate et al. 2015; Liu et al. 2016; Fu 2017).

The functionality of μPADs is based on the ability of paper to transport liquid passively due to capillary action in regions where the imbibed fluid undergoes a kind of chemical analysis. Hence, the majority of current research focuses on: (1) advanced fabrication techniques for accurate control of imbibition dynamics, which include effects of paper geometry (Elizalde et al. 2015; Walji and MacDonald 2016), repeated wettings (Elizalde et al. 2016), humidity (Castro et al. 2017), fibre nature (Böhm et al. 2014), hydrophobic patterning and wax boundaries (Hong and Kim 2015; Koivunen et al. 2016), use of programmable devices that include 3D paper channels (Li and Liu 2014), as well as on (2) the principal functionality of μPADs, which is the ability to quantify the analyte.

The most common detection method is based on colorimetric approaches, e.g. Dungchai et al. (2010); Evans et al. (2014), where the colour intensity of the wetted paper is proportional to analyte concentration. This is based on enzymatic or chemical colour change reactions, while the compatibility of such devices with modern smartphone cameras (Il Hong and Chang 2014; Wu et al. 2017) facilitates a portable diagnostic procedure. Colorimetric methods have been used for glucose detection in urinalysis (Gabriel et al. 2016; Tarso et al. 2014), tear electrolyte analysis (Yetisen et al. 2017), paraquat poisoning in human serum (Kuan et al. 2016) as well as blood separation (Songjaroen et al. 2012). However, different light conditions provide inconsistent image intensities limiting the usage in real-world applications (Yamada et al. 2017; Morbioli et al. 2017). Increased sensitivity has been achieved by coupling μPADs with electrochemical readers (Noiphung et al. 2013; Lankelma et al. 2012; Nie et al. 2010), while distance-based detection

✉ A. Terzis
alexandros.terzis@me.com

[1] Institute of Aerospace Thermodynamics (ITLR), University of Stuttgart, Pfaffenwaldring 31, 70569 Stuttgart, Germany

[2] Environmental Hydrogeology Group, Department of Earth Sciences, University of Utrecht, 3584 CD Utrecht, The Netherlands

[3] Laboratorio de Fluidodinámica, Facultad de Ingeniería UBA, CONICET, Buenos Aires, Argentina

[4] School of Engineering, Aristotle University of Thessaloniki, 54124 Thessaloníki, Greece

[5] Institute for Personalised Medicine, School of Biomedical Engineering, Shanghai Jiao Tong University, 200030 Shanghai, China

methods have been also reported (Cate et al. 2013; Li et al. 2014; Elizalde et al. 2016), where the concentration of the analyte is related to the travelled distance of the imbibed liquid.

The diagnostic method we are presenting here is based on the temporal heat release at a wetting front during spontaneous imbibition. Such temperature spikes have been initially suggested as a detector for solid–liquid chromatography in late 1950s (Claxton 1959) and they have been also observed during infiltration of dry soils (Anderson and Linville 1960). However, Terzis et al. (2017) indicated that the released heat can be enormous for the given scale of μPADs and related the level of temperature rise to the energetics of imbibition compounds. The objective of this work is to show that the temperature rise can be associated with a prospective liquid concentration demonstrating a great potential for quantitative paper-based microfluidics.

2 Results

2.1 Introductory remarks

The test setup is described in Terzis et al. (2017); thus, only a brief overview will be given here. All experiments were carried out using an uncoated and chemically untreated paper (Löschblätter Art. 10-41 546, BRUNNEN), as shown in Fig. 1. The scanning electron images and X-ray diffraction analysis of the material revealed an average fibre size of 12 μm and its purely cellulosic character. The paper strips have 231 μm thickness, 140 g/m^2 weight per area and a porosity of 0.59. In order to eliminate liquid evaporation from the wetted paper, its front surface was covered with a clear polypropylene tape that is also transparent to infrared radiation. The liquid bath was set at room temperature, and once isothermal conditions were obtained, it was vertically transversed to force imbibition against gravity. Optical and thermal images were recorded at 4 Hz to quantitatively visualise the liquid invasion process.

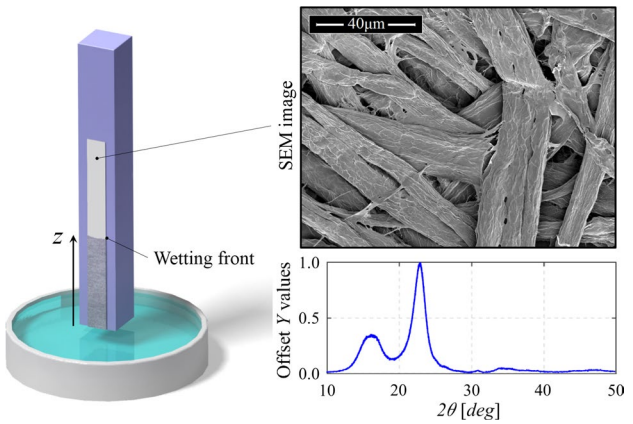

Fig. 1 Schematic illustration of experimental setup and characterisation of paper substrate by scanning electron microscopy (SEM) and X-ray diffraction (XRD) analysis. In the XRD patterns, the characteristic diffraction peaks of cellulose are observed for 16.5°, 22.7° and 34.2°. SEM images were obtained on a FEI Nova Nano 450 operating at 5 kV. XRD patterns obtained using a Bruker D8 Advance (*CuKa*, 40 kV, 40 mA)

2.2 Capillary thermodynamics of aqueous urea solutions

Figure 2 shows optical and thermal images of the imbibition process for two aqueous urea solutions with urea concentration of 16.6 and 33.3% (w/w). The 16.6% solution propagates faster, and this is directly reflected in Washburn's equation, $z(t) \sim \sqrt{\gamma_l/\mu}$ (Washburn 1921). Although both the dynamic viscosity (μ) and surface tension (γ_l) increase with urea mass fraction, the influence on μ is more pronounced (Halonen et al. 2016) decelerating the wicking rates.

Regarding the released heat, for both solutions the temperature is temporarily increased at the interface between the wetting and the non-wetting phases, while the level of heat release is gradually reduced at later imbibition stages where the liquid front becomes more diffusive and hence less saturated (Helmig 1997). However, the temperature rise is higher for x_i=16.6% over the complete length of the paper.

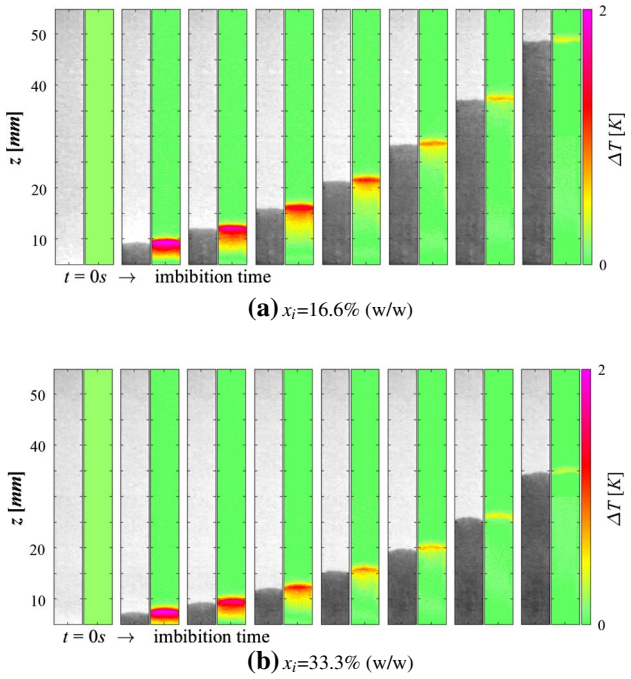

Fig. 2 Optical (black and white) and thermal (colour) images of urea–water solution spontaneous imbibition. Consecutive frames are displayed in a logarithmic time scale. The paper strips are cut in $5 \times 50(\text{mm})^2$

Figure 3 shows that ΔT at $z = 20$ mm is about 0.5 K higher for x_i =16.6%, while thermal spike is similar to that observed in solidification fronts inside sessile drops (Schmid et al. 2018). The figure also shows the similar wettability of the solutions on a low energy and nearly apolar PDMS (polydimethylsiloxane) surface. The contact angle is just slightly reduced for $x_i = 33.3\%$ indicating the more apolar nature of the solution at higher mass fractions, in agreement with Terzis et al. (2018). Therefore, the released energy cannot only be attributed to the heat of wetting on the slightly polar cellulosic surface. Terzis et al. (2017) related the level of temperature rise to the energetics of imbibition compounds, as an acid–base neutralisation reaction.

Cellulose is known to be characterised by a significant electron-donor capacity (Dourado et al. 2012), while Terzis et al. (2018) indicated that as urea concentration increases, the electron donating behaviour of the solution is also enhanced. Table 1 summarises typical energetic characteristics for cellulose and urea–water solutions, including their acid-based contributions. As urea concentration increases, the paper and the imbibed liquid become energetically more similar. Hence, any charge transfer or neutralisation reaction at the interface is less intense. Since the interfacial energy between two energetically similar surfaces is zero, this means that the released heat at the wetting front can be related to the energetic dissimilarity between the compounds involved.

Table 1 Surface energy components of urea–water solutions (Terzis et al. 2018) and cellulose (Van Oss 2006) at 25 °C

	γ	γ^{LW}	γ^{AB}	γ^{+}	γ^{-}
Cellulose	41.47	40.00	4.47	0.10	50.00
UWS 0%	71.94	21.27	50.66	25.33	25.33
UWS 16.6%	72.76	25.62	47.13	20.59	26.97
UWS 33.3%	73.67	27.95	45.71	19.30	27.06
UWS 50%	74.99	31.29	43.69	16.97	28.11

Values are in mJ/m^2

The capillary dynamics of urea–water solutions is shown in Fig. 4a where the imbibition rate is significantly reduced as urea concentration increases. This is due to the considerable increase in dynamic viscosity, which is twice the value of pure water for $x_i = 50\%$. Figure 4b shows for various travelled distances, how the local ΔT varies with urea mass fraction. Pure water provides the maximum thermal peak due to the strong hydrogen bonding with the available hydroxyls (OH^-) of the fibre surfaces. However, Terzis et al. (2018) showed that the polarity of the solution decreases with urea concentration, and thus, the hydrogen bond opportunities with the fibre surfaces should be also reduced. Indeed, for a 50% (w/w) solution, the local ΔT is reduced from 2.35 to 1.26 K at $z = 10$ mm (− 46.3%) and from 1.25 to 0.41 K for $z = 25$ mm (− 67.2%). This shows also that the influence of urea on the released energy is more pronounced at higher imbibition lengths. The latter can be associated with the stronger adsorption capacity of water molecules on the cellulose that results in higher urea concentrations at later imbibition stages. A direct relation of temperature

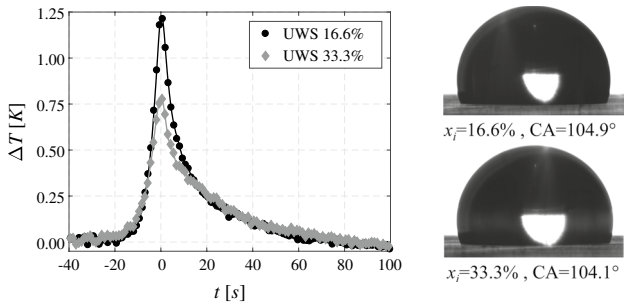

Fig. 3 Temperature spikes at the wetting front for two urea–water solutions (UWS) at $z = 20$ mm and contact angles (CA) on a PDMS surface. std = ± 0.08 °C

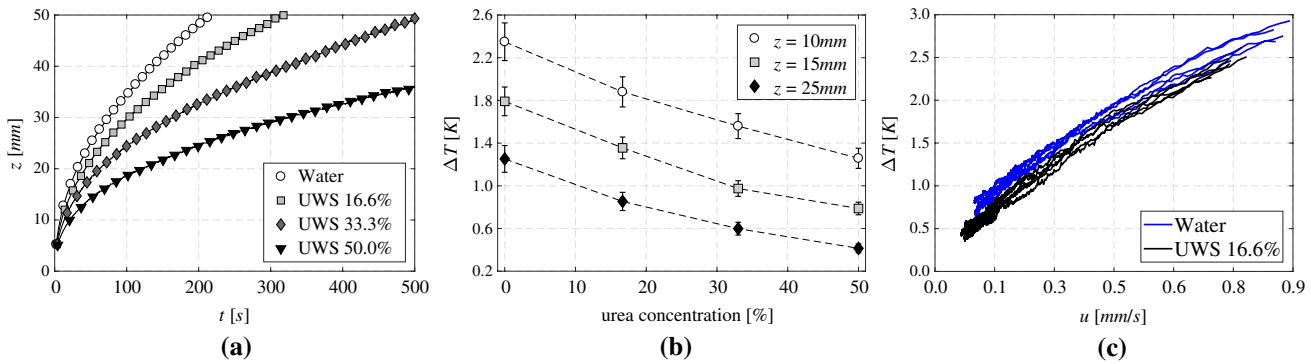

Fig. 4 **a** Capillary dynamics of various urea–water solutions (UWS), **b** local temperature rise at the wetting front as a function of urea concentration at various imbibition heights and **c** average temperature rise for the complete wetting of the paper

rise with the imbibition speed is indicated in Fig. 4c which shows five individual experiments using distilled water and a 16.6% aqueous solution. For a given wetting front speed, water provides higher temperature rise which indicates that the differences in the released heat are due to the presence of the analyte. Furthermore, the influence of urea is more intense when the wicking velocity is slow (higher imbibition heights). In particular, the obtained temperature rise for water is about 38 and 8% higher when the imbibition velocity is 0.1 and 0.8 mm/s, respectively.

2.3 Influence of paper size

Figure 5 shows image-pair snapshots of pure water imbibition at 40 s and various paper sizes. The first three image pairs show a single paper layer of 4, 6 and 8 mm width. In general, the travelled distance of water is observed to be reduced for narrower channels in agreement with Castro et al. (2017). Although an opposite trend in the literature has been also observed (Böhm et al. 2014; Walji and MacDonald 2016), the imbibition dynamics in this study is additionally influenced by the transparent polypropylene tape on the front and side surfaces of the paper. This generates hydrophobic boundaries which are able to retard imbibition dynamics since the interfacial tension in these regions acts in an inverse direction to the flow (Hong and Kim 2015). Interestingly, the influence of paper width is significantly reflected in the thermal images since the temperature rise increases for wider channels. This is probably related to the higher influence of the hydrophobic boundaries that reduce the saturation of the wetting front. The last two image pairs show a double and a quadruple layer of a 6 mm paper width. The imbibition speed increases with the overall thickness of the substrate; however, the effect is less pronounced for a quadruple layer. This could be attributed to an imperfect packing of the individual paper strips. In order to truly evaluate paper thickness effects, individual strips made of different thicknesses, instead of multi-layer packing, should be used. Nevertheless, there is a substantial increase in the released heat since the thermal peak for the quadruple paper exceeds 4.5 K. For multi-layer paper samples, similar findings were also reported by Aslannejad et al. (2017).

Figure 6 summarises all experiments performed with water (including paper strips that are not present in Fig. 5) and shows that the average temperature rise for the complete wetting of the paper increases almost linearly with the substrate cross section (width × thickness). This is due to the larger interfacial area between the fluid and the porous platform for thicker papers and due to the smaller influence of hydrophobicity in the boundaries for wider channels. The latter has a direct influence on the saturation of the wetting front as well as the heat losses in the side boundaries.

2.4 Artificial urine samples

The applicability of biological fluids to produce a temperature rise at the wetting front has been also examined using artificial urine solutions produced according to DIN EN 1616:1999, while glucose was selected as the specific analyte for identification. Similar to cellulose, glucose is also characterised by a significant electron-donor capacity (Van Oss 2006), which means that the higher the glucose concentration is, the more energetically compatible are the cellulosic platform and the imbibed liquid. Hence, the temperature spikes should be reduced. Indeed, Fig. 7c shows that the average temperature rise for the complete wetting of the paper is reduced with increasing glucose concentration. However, the detectable level of glucose does not represent realistic applications, since typical values in human urine are less than 30 mM. Nevertheless, Fig. 7 demonstrates a very clear monotonic trend where proper patterning of the cellulosic platform with appropriate reagents might enhance the thermal sensitivity in various concentrations.

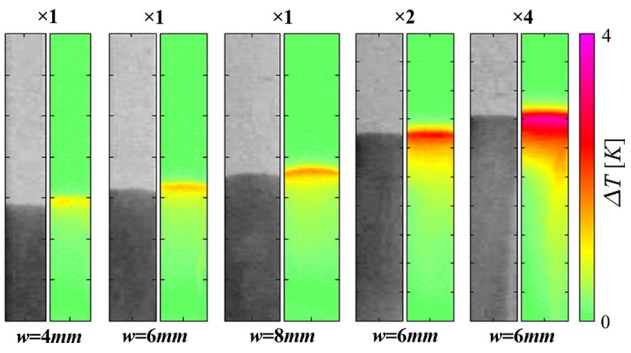

Fig. 5 Optical and thermal images of water imbibition for various paper sizes. The images are displayed 40 s after the initiation of imbibition

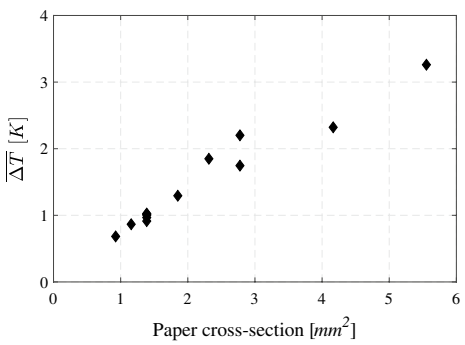

Fig. 6 Average temperature rise over the complete length of paper substrates as a function of imbibition paper cross section

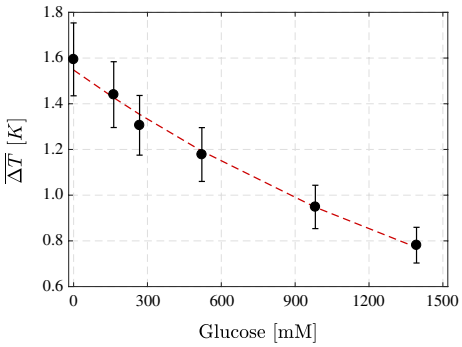

Fig. 7 Glucose level detection based on the average temperature rise during the complete wetting of $5 \times 35(\text{mm})^2$ paper strip. The error bars correspond to the uncertainty of five individual experiments

3 Concluding remarks

In this brief communication, we presented the potential of a temperature-based quantitative diagnostic approach for paper-based microfluidics, inspired by the thermal spikes observed at the wetting front during capillary filling of cellulosic materials (Terzis et al. 2017). The applicability of biological fluids was examined, and the obtained temperature rise at the liquid front was successfully related to the concentration of specific analytes, such as urea (in aqueous solutions) and glucose (in artificial urine). Although the detectable concentrations do not represent realistic levels, we believe that the monotonic trend that can be achieved as well as proper patterning of the cellulosic platform with appropriate reagents, will result in a more sensitive response of a temperature sensor according to different analyte concentrations. The temperature rises can be enormous for the given length scale of μPADs exceeding locally 3 K for a purely cellulosic substrate. This demonstrates a great potential for future, rapid and quantitative diagnostics for paper-based microfluidics.

Acknowledgements A. Terzis acknowledges the support of Alexander von Humboldt (AvH) foundation. I. Zarikos acknowledges the support received under the ERC Grant Agreement No. 341225. Special thanks go to Dr. Eleftheria Roumeli (California Institute of Technology) for characterizing the paper samples. The authors are also grateful to Prof. S. Majid Hassanizadeh (Utrecht University) for his overall contribution.

References

Anderson DM, Linville A (1960) Temperature fluctuations accompanying water movement through porous media. Science 131(3410):1370–1371

Aslannejad H, Terzis A, Hassanizadeh SM, Weigand B (2017) Occurrence of temperature spikes at a wetting front during spontaneous imbibition. Sci Rep 7(1):7268

Böhm A, Carstens F, Trieb C, Schabel S, Biesalski M (2014) Engineering microfluidic papers: effect of fiber source and paper sheet properties on capillary-driven fluid flow. Microfluid Nanofluid 16(5):789–799

Castro C, Rosillo C, Tsutsui H (2017) Characterizing effects of humidity and channel size on imbibition in paper-based microfluidic channels. Microfluid Nanofluid 21(2):21

Cate DM, Adkins JA, Mettakoonpitak J, Henry CS (2015) Recent developments in paper-based microfluidic devices. Anal Chem 87(1):19–41

Cate DM, Dungchai W, Cunningham JC, Volckens J, Henry CS (2013) Simple, distance-based measurement for paper analytical devices. Lab Chip 13(12):2397–2404

Claxton G (1959) Detector for liquid–solid chromatography. J Chromatogr A 2:136–139

de Tarso Garcia P, Cardoso TMG, Garcia CD, Carrilho E, Coltro WKT (2014) A handheld stamping process to fabricate microfluidic paper-based analytical devices with chemically modified surface for clinical assays. RSC Adv 4(71):37637–37644

Dourado F, Gama FM, Chibowski E, Mota M (2012) Characterization of cellulose surface free energy. J Adhes Sci Technol 12(10):1081–1090

Dungchai W, Chailapakul O, Henry CS (2010) Use of multiple colorimetric indicators for paper-based microfluidic devices. Anal Chim Acta 674(2):227–233

Elizalde E, Urteaga R, Berli CLA (2015) Rational design of capillary-driven flows for paper-based microfluidics. Lab Chip 15(10):2173–2180

Elizalde E, Urteaga R, Berli CLA (2016) Precise capillary flow for paper-based viscometry. Microfluid Nanofluid 20(10):135

Evans E, Gabriel EFM, Coltro WKT, Garcia CD (2014) Rational selection of substrates to improve color intensity and uniformity on microfluidic paper-based analytical devices. Analyst 139(9):2127–2132

Fu E, Downs C (2017) Progress in the development and integration of fluid flow control tools in paper microfluidics. Lab Chip 17:614

Gabriel EFM, Garcia PT, Cardoso TMG, Lopes FM, Martins FT, Coltro WKT (2016) Highly sensitive colorimetric detection of glucose and uric acid in biological fluids using chitosan-modified paper microfluidic devices. Analyst 141(15):4749–4756

Halonen S, Kangas T, Haataja M, Lassi U (2016) Urea-water-solution properties: density, viscosity, and surface tension in an undersaturated solution. Emiss Control Sci Technol 3(2):161–170

Helmig R (1997) Multiphase flow and transport processes in the subsurface. Springer, Berlin

Hong S, Kim W (2015) Dynamics of water imbibition through paper channels with wax boundaries. Microfluid Nanofluid 19(4):845–853

Il Hong J, Chang B-Y (2014) Development of the smartphone-based colorimetry for multi-analyte sensing arrays. Lab Chip 14(10):1725–1732

Koivunen R, Jutila E, Bollström R, Gane P (2016) Hydrophobic patterning of functional porous pigment coatings by inkjet printing. Microfluid Nanofluid 20(6):83

Kuan C-M, Lin S-T, Yen T-H, Wang Y-L, Cheng C-M (2016) Paper-based diagnostic devices for clinical paraquat poisoning diagnosis. Biomicrofluidics 10(3):034118

Lankelma J, Nie Z, Carrilho E, Whitesides GM (2012) Paper-based analytical device for electrochemical flow-injection analysis of glucose in urine. Anal Chem 84(9):4147–4152

Li H, Han D, Pauletti GM, Steckl AJ (2014) Blood coagulation screening using a paper-based microfluidic lateral flow device. Lab Chip 14(20):4035–4041

Li X, Liu X (2014) Fabrication of three-dimensional microfluidic channels in a single layer of cellulose paper. Microfluid Nanofluid 16(5):819–827

Liu S, Su W, Ding X (2016) A review on microfluidic paper-based analytical devices for glucose detection. Sensors 16(12):2086

Martinez AW, Phillips DST, Butte DMJ, Whitesides PGM (2007) Patterned paper as a platform for inexpensive, low volume, portable bioassays. Angew Chem (Int Engl) 46(8):1318–1320

Martinez AW, Phillips ST, Whitesides GM, Carrilho E (2010) Diagnostics for the developing world: microfluidic paper-based analytical devices. Anal Chem 82(1):3–10

Morbioli GG, Mazzu-Nascimento T, Stockton AM, Carrilho E (2017) Technical aspects and challenges of colorimetric detection with microfluidic paper-based analytical devices (μPADs) - A review. Anal Chim Acta 970:1–22

Nie Z, Deiss F, Liu X, Akbulut O, Whitesides GM (2010) Integration of paper-based microfluidic devices with commercial electrochemical readers. Lab Chip 10(22):3163–3169

Noiphung J, Songjaroen T, Dungchai W, Henry CS, Chailapakul O, Laiwattanapaisal W (2013) Electrochemical detection of glucose from whole blood using paper-based microfluidic devices. Anal Chim Acta 788:39–45

Schmid J, Zarikos I, Terzis A, Roth N, Weigand B (2018) Crystallization of urea from an evaporative aqueous solution sessile droplet at sub-boiling temperatures and surfaces with different wettability. Exp Therm Fluid Sci 91:80–88

Songjaroen T, Dungchai W, Chailapakul O, Henry CS, Laiwattanapaisal W (2012) Blood separation on microfluidic paper-based analytical devices. Lab Chip 12(18):3392–3398

Terzis A, Roumeli E, Weishaupt K, Brack S, Aslannejad H, Groß J, Hassanizadeh SM, Helmig R, Weigand B (2017) Heat release at the wetting front during capillary filling of cellulosic microsubstrates. J Colloid Interface Sci 504:751–757

Terzis A, Sauer E, Yang G, Groß J, Weigand B (2018) Characterisation of acid–base surface free energy components of urea–water solutions. Colloids Surf A Physicochem Eng Asp 538:774–780

VanOss CJ (2006) Interfacial forces in aqueous media, 2nd edn. CRC Press, Boca Raton

Walji N, MacDonald B (2016) Influence of geometry and surrounding conditions on fluid flow in paper-based devices. Micromachines 7(5):73

Washburn EW (1921) The dynamics of capillary flow. Phys Rev 17(3):273–283

Wu D, Zhang J, Xu F, Wen X, Li P, Zhang X, Qiao S, Ge S, Xia N, Qian S, Qiu X (2017) A paper-based microfluidic Dot-ELISA system with smartphone for the detection of influenza A. Microfluid Nanofluid 21(3):43

Yager P, Edwards T, Fu E, Helton K, Nelson K, Tam MR, Weigl BH (2006) Microfluidic diagnostic technologies for global public health. Nature 442(7101):412–418

Yamada K, Shibata H, Suzuki K, Citterio D (2017) Toward practical application of paper-based microfluidics for medical diagnostics: state-of-the-art and challenges. Lab Chip 21:1123

Yetisen AK, Akram MS, Lowe CR (2013) Paper-based microfluidic point-of-care diagnostic devices. Lab Chip 13(12):2210–2251

Yetisen AK, Jiang N, Tamayol A, Ruiz-Esparza GU, Zhang YS, Medina-Pando S, Gupta A, Wolffsohn JS, Butt H, Khademhosseini A, Yun S-H (2017) Paper-based microfluidic system for tear electrolyte analysis. Lab Chip 28:1250